Macromolecules

pubs.acs.org/Macromolecules Article

Localized and Collective Dynamics in Liquid-like Polyethylenimine-Based Nanoparticle Organic Hybrid Materials

Emmanuel Urandu Mapesa, Nelly M. Cantillo, Sara T. Hamilton, Matthew A. Harris, Thomas A. Zawodzinski, Jr.,* Ah-Hyung Alissa Park,* and Joshua Sangoro*

Cite This: https://dx.doi.org/10.1021/acs.macromol.0c02370 Read Online

ACCESS | Metrics & More | Article Recommendations | Supporting Information

ABSTRACT: Broadband dielectric spectroscopy, rheology, and nuclear magnetic resonance spectroscopy are employed to study molecular dynamics in a nanoparticle organic hybrid material (NOHMs) system comprising 20 wt % silica nanoparticles ionically bonded to a polyethylenimine canopy. By comparing the neat polymer (used as a canopy) to the derivative NOHMs, we find that timescales characterizing segmental dynamics in the NOHM are identical to those for the neat polymer. Detailed analysis of the carbon-spin lattice relaxation times yields mechanistic insights into localized and collective dynamics, in quantitative agreement with dielectric results. Interestingly, the NOHMs retain liquid-like characteristics unlike conventional polymer nanocomposites but exhibit higher viscosity due to additional contributions from tethered polymer chains and mesoscopic structuring. These findings demonstrate the potential of achieving unique and desired material properties *via* NOHMs by an informed choice of the canopy material.

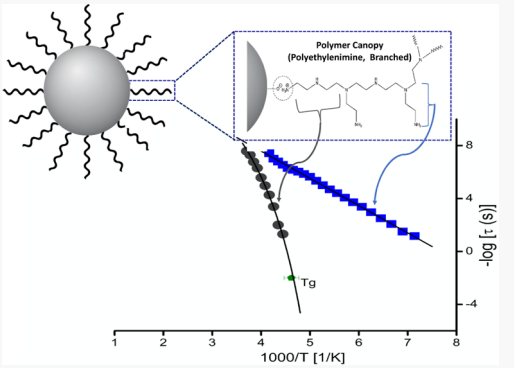

INTRODUCTION

Nanoparticle organic hybrid materials (NOHMs)—especially those that are typically solvent-free fluids—have attracted research and engineering interest because of the great potential they hold for diverse applications, for instance, as conductive lubricants,[1−5] magnetic fluids,[6,7] novel reaction solvents,[8−13] thermal control materials,[14−20] and nanocomposite materials.[21,22] The fact that these NOHMs retain liquid-like properties at room temperature means that they can be designed to combine desired characteristics of liquids, for example, photoluminescence with the attributes of the core nanostructures such as high mechanical modulus. The parameter space that can be tweaked to obtain NOHMs with desired properties is wide as it encompasses composition, structure, and chemistry. More specifically, millions of possible variations of these materials can be synthesized by tuning the shape and size of the core, length and composition of the corona, and composition and molecular weight of the canopy. There is no doubt therefore that the extent to which NOHMs can be engineered to meet specific requirements depends on in-depth understanding of the role played by each of their structural components in determining the overall properties. Among the applications for which NOHMs are outstanding as potential candidates is their use as novel solvents for gas separations, particularly CO_2 capture.[11−13,23−28] Since they are chemically and thermally stable and possess negligible vapor pressure with high degrees of chemical and physical tunability, they are promising for a wide range of reactive and separation systems. NOHMs have been found to interact with gas molecules and ionic species based on enthalpic contributions, which arise from the functional groups along the tethered polymeric chains as well as entropic contributions, which are driven by the structural configurations of the polymeric canopy.[12] The introduction of amine functional groups along the polymer chains in NOHM-I-PEI results in a high CO_2 capture capacity (2.4 mmol of CO_2 per gram of solvent at 30 °C and 3.4 atm[13]), which is comparable to that of pure monoethanolamine. NOHMs have recently been found to be useful as electrolyte additives with controlled chemical affinities toward target species. Thus, NOHM-I-PEI-based electrolytes have been developed for combined CO_2 capture and electrochemical conversion where NOHMs can significantly increase CO_2 solubility in the electrolyte and even serve as a cocatalyst.[29] In a recent study by some of the current authors, NOHM-I-PEI was explored as an electrolyte additive for a flow battery.[30] This study focused on how the amine functional groups of NOHM-I-PEI can strongly chelate redox active species (*e.g.,* Cu(II)) and increase the solubility of Cu in the flow battery. The electrochemical behavior of the NOHM-

Received: October 19, 2020
Revised: February 8, 2021

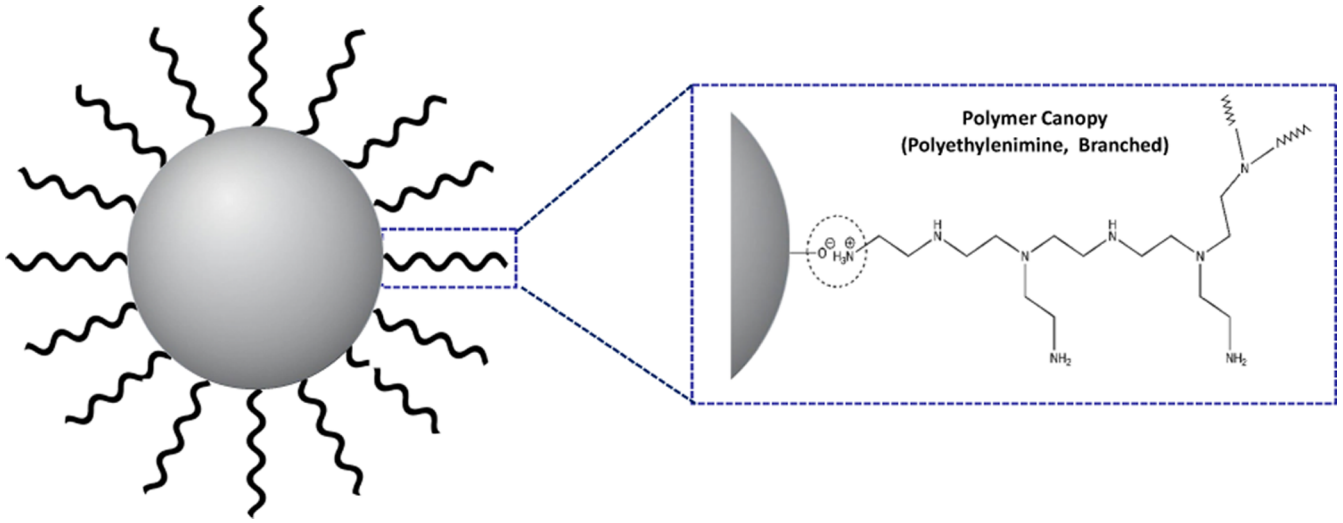

Figure 1. Schematic representation of the structure of the hybrid material, NOHM-I-PEI whose canopy is branched polyethylenimine (PEI), ionically bonded to a silica core.

I-PEI/Cu(II) complexes as well as the effect of the pH on the extent of cation binding by NOHMs was investigated.

One of the key properties of these hybrid materials that demand concise characterization is their molecular dynamics since they determine the temperature and size ranges in which desired innovations can be achieved. In their quest to understand canopy dynamics, Jespersen *et al.* applied nuclear magnetic resonance (NMR) to probe hybrid materials made from silica cores modified by an alkylsilane monolayer with sulfonic acid functionality, bearing an amine-terminated block copolymer (ethylene oxide/propylene oxide) canopy.[31] They show that the diffusion of the canopy in the hybrid slowed relative to the neat polymer but not to the degree predicted by considering diffusion of hard-sphere particles. Focusing their attention on the role of constituent components, Bourlinos *et al.* studied ionically modified silica nanoparticles with large sulfonate (and isostearate) counter anions.[32] They demonstrate that glass transition temperature is governed by the large counter anions while flow properties hinge on the spatial correlation between the nanoparticles. So far, a systematic study of the dynamics in the neat canopy and the consequent hybrid material is lacking. The interplay between the structure and the local as well as collective dynamics in the NOHMs remains unclear. In order to advance the understanding as well as engineering possibilities in the fast-emerging field of NOHMs, it is imperative that fundamental studies of this kind be pursued.

In the present work, rheology, carbon-nuclear magnetic resonance (carbon-NMR), and broadband dielectric spectroscopy (BDS) are employed to study collective and localized dynamics in a NOHM whose highly branched polyethylenimine (PEI) canopy is ionically bonded to a core of silica nanoparticles (the hybrid material is referred to as NOHM-I-PEI in the rest of this article)—see Figure 1. For completeness, the neat canopy material, PEI, is also characterized. It is shown that both segmental and secondary structural relaxations in PEI are identical to those in NOHM-I-PEI, but the hybrid material exhibits higher viscosity. Carbon-NMR relaxation results also show that the fast (ns) dynamics are not influenced by the presence of the silica cores. The local motion is found to be reduced for the methylene groups located in the "interior" of the polymer canopy in both PEI and NOHM-I-PEI while the relaxation of methylene groups located in the extremities of the canopy (either side or end chain) shows good agreement with the β-process identified from the BDS analysis. Put together, our results demonstrate the key roles played by the inorganic core and polymeric canopy in determining the local and collective dynamics in these hybrid materials.

MATERIALS AND METHODS

Synthesis of NOHM-I-PEI. NOHM-I-PEI employed in this work was prepared as described in previous studies.[13,30] As briefly described, a colloidal silica suspension (7 nm diameter, Ludox SM-30 Sigma-Aldrich) was diluted to 3 wt. % and a cation exchange column (DOWEX Marathon C, Sigma-Aldrich) was employed to replace the sodium ions on the nanoparticle surface with protons. This surface-protonated silica suspension was mixed with a dilute solution of polyethylenimine, branched (Branched, M.W. 2000, Polyscience Inc.) to achieve the desired polymer canopy to silica core mass ratio of 80:20. The PEI has a molecular weight of 2000 g/mol and a density of 1.05 g/cm^3, as reported by the manufacturer. It contains primary, secondary, and tertiary amines in an approximate ratio of 40/36/24, as reported. Dynamic light scattering (DLS) was used to determine the average hydrodynamic diameter of PEI in dilute solution, which is found to be 2.19 nm. The sample is found to have a narrow size distribution—see Figure S1 in the Supporting Information. Thermal gravimetric analysis was used for confirmation of ionic bond formation.

Differential Scanning Calorimetry. Heat flow measurements were performed using differential scanning calorimetry (DSC) 214 Polyma (NETZSCH). 10.0 mg of sample (NOHM-I-PEI and PEI) was weighted in a 40 μL 6 mm Al standard crucible with a pinhole. Samples were cycled between −80and 100 °C at a rate of 10 K/min for six scans. An empty aluminum pan was used as a reference. The glass transition temperature (T_g) was determined from the DSC measurements. Both the unbound polymer (PEI) and the tethered polymer (NOHM-I-PEI) were found to have similar T_gs of −60 ± 3 °C. The transition is observed to be broader in the neat polymer than the hybrid system (Figure S2) and is discussed later.

Rheology. Rheology measurements were performed using a TA Instruments Discovery Hybrid Rheometer (HR2) in small-amplitude oscillatory shear (SAOS) mode using 3 mm stainless steel parallel plates. The real and imaginary parts of the complex shear modulus and the complex viscosity were recorded at various temperatures between −60 and −30 °C controlled within 0.1 °C of the set point using a liquid nitrogen coolant. The data was processed using TA

https://dx.doi.org/10.1021/acs.macromol.0c02370
Macromolecules XXXX, XXX, XXX−XXX

Instruments TRIOS software to produce master curves and shift factors based on time−temperature superposition.

X-ray Scattering. Small- and wide-angle X-ray scattering measurements were performed using a SAXSLAB Ganesha instrument equipped with a Cu Kα 50 kV Xenocs GeniX ULD SL X-ray source (beam energy of 8 keV) and a 170 μm pixel-spaced, single photon counting Dectris Pilatus 300k 20 Hz detector. Quartz capillary tubes of 1 mm in diameter were filled with the samples and sealed prior to loading into the instrument. Additional samples were prepared by placing a drop of the polymer or NOHM between strips of Kapton tape. A blank measurement was performed on the Kapton tape without the sample included. Small-angle X-ray scattering (SAXS) and wide-angle X-ray scattering (WAXS) data were collected at room temperature under vacuum in the q-range from 0.002 to 2.6 Å^{-1}.

Nuclear Magnetic Resonance. Neat samples of both the untethered free PEI polymer and the NOHM-I-PEI were transferred in a standard 5 mm NMR tube. Previously, both samples were dried under vacuum at 50 °C for 3 h to remove residual water from the neat sample. ^{13}C NMR spectra were recorded on a Bruker Avance III 400 WB spectrometer, operating at 100.61 MHz with a temperature controller. The ^{13}C spin−lattice relaxation time (T_1) spectra were measured using the inversion-recovery method with a set of 16 recovery (τ) periods. For each τ value, the number of repetitive scans was set to 256. The relaxation delay was at least 5 T_1 plus the acquisition time. The τ values were varied up to 1.5 T_1. The spectra were phase-corrected, and T_1 values were calculated from the signal intensity data using MestreNova. All carbon atoms present in the molecule have at least one directly bonded hydrogen.

Broadband Dielectric Spectroscopy. BDS experiments were performed on a high-resolution Alpha analyzer equipped with a Quatro system with the capability to control temperature within 0.1 K of the set point (from Novocontrol Technologies GmbH). Polymer and the NOHM samples were sandwiched between two polished brass electrodes (diameter, 15 mm) forming a parallel-plate capacitor configuration. The sample thickness was maintained using 100 μm thick silica spacers. Before substantive dielectric measurements, the films were annealed at 420 K under inert conditions ensured by dry nitrogen flow for ∼8 h in order to remove any adsorbed water. During this annealing process, the real part, ε', of the complex permittivity was monitored as a function of time. ε' increases to a maximum value as the set temperature point is reached and eventually decays to a plateau value after several hours of annealing. Dielectric measurements were carried out in the frequency range 1 mHz to 10 MHz over cooling and heating cycles between 140 and 400 K.

RESULTS AND DISCUSSION

X-ray scattering data for both the PEI and NOHM-I-PEI are displayed in Figure 2. Assuming a simple form factor model for monodisperse spheres (see Figure S3), a diameter of ∼10.4 nm (*i.e.*, correlation distance, d_1) (or radius, d_2 ∼ 5.2 nm) is found for the nanoparticles. Given that the diameter of the nanoparticles is 7 nm, the spacing between them is more than that; hence, this finding from SAXS is consistent with the expectation. The correlation distance d_3 ∼ 1.4 nm as observed (inset [a], Figure 2) in the medium-angle X-ray scattering (MAXS) region—and independently confirmed by wide-angle X-ray scattering measurements (inset [b], Figure 2)—is present in the hybrid material but not the neat polymer. We conjecture that because of the presence of nanoparticles, there is some degree of mesoscale organization in the polymeric regions of the NOHM leading to aggregates whose size is about 1.4 nm. We shall revisit this idea in the discussion of the dynamics results. Finally, because d_4 ∼ 0.45 nm is observed in both PEI and NOHM-I-PEI, it must be an intrinsic character of the polymer, very likely the backbone-to-backbone separation.[33] It is instructive to note that there is a slight broadening in the peak for the NOHM compared to that of the

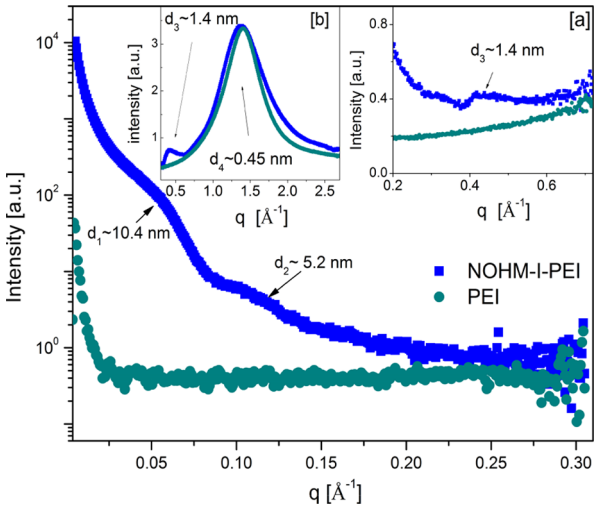

Figure 2. Experimentally determined small-angle X-ray scattering (SAXS) data for NOHM-I-PEI (blue symbols) and PEI (dark gray symbols), showing various correlation distances estimated from the peak position as $d_i = 2\pi/q$. The insets [a] and [b] show the corresponding medium-angle (MAXS) and wide-angle X-ray scattering (WAXS) profiles.

polymer (inset [b], Figure 2). This is consistent with the expectation that polymer−nanoparticle interactions lead to disruptions in the packing of the polymer chains.

A visual inspection of PEI and NOHM-I-PEI samples shows that the two samples have distinct flow properties. The flow characteristics of non-Newtonian fluids can be accounted for using rheology, which typically probes the relationship between the stress and rate of change of strain. Figure 3

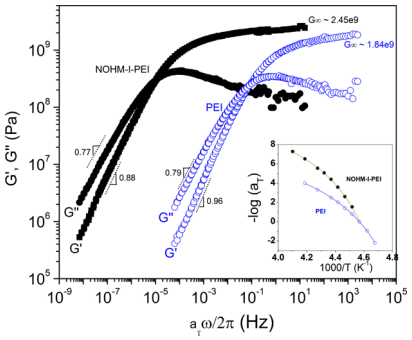

Figure 3. Master curves (reference temperature, −55 °C) showing the real (G') and imaginary (G'') parts of the complex shear modulus, G^*, for PEI (empty circles) and NOHM-I-PEI (filled squares). Inset: shift factors used to construct the master curves. The solid lines are fits to the VFT equation. The fit parameters are provided in the caption of Figure S4. The error bars are comparable to the size of the symbols unless otherwise indicated.

shows master curves of the real (G') and imaginary (G'') parts of the complex shear modulus (G^*) for PEI (circles) and NOHM-I-PEI (squares) and the shift factors (see inset) used to construct them. The construction of master curves was achieved by employing the time−temperature superposition principle, where the dynamic loss and storage moduli measured over a range of oscillatory frequencies at several discrete temperatures are shifted to a fixed temperature of −55 °C by multiplying the frequency axis with a temperature-dependent factor, a_T. From Figure 3, we observe that G' and

https://dx.doi.org/10.1021/acs.macromol.0c02370
Macromolecules XXXX, XXX, XXX−XXX

G'' intersect at different oscillatory frequencies for the two materials. This implies, *inter alia*, that the fundamental relaxations responsible for mechanical energy dissipation in the two systems have different time scales ($\sim 10^2$ and $\sim 10^5$ s at −55 °C). Interestingly, the frequency-scale shift factors for the two materials are not identical both in their absolute values and—more significantly—their temperature dependence (see inset, Figures 3 and S4). This difference precludes the possibility that a single identical relaxation process controls the mechanical energy dissipation in the two materials. We note here that while some studies[34,35] have observed two crossover points for G' and G'' and explained this in terms of time and temperature enhancement of corona chain interpenetration, some other investigations of comparable hybrid systems do not make this observation;[32,36] this is an open question for further research. The mean relaxation times obtained from rheology coincide with those of the structural relaxation for PEI as determined from BDS measurements (Figure 6); this means that the structural relaxation controls the mechanical response in the neat polymer. However, the mean times from rheology for NOHM-I-PEI are substantially slower than those dielectrically determined for the structural process. Effectively, therefore, longer range motions than the α-process affect the rheological response in the hybrid material. It is possible to think of the fundamental times reported by rheology for the NOHM material to be influenced by the characteristic times for the motion of the silica particles in a liquid medium where the viscosity is set by the tethered PEI chains and the characteristic length scale is largely controlled by interparticle interaction. Indeed, it has been demonstrated that small nanoparticles contribute to the structural relaxation in composite systems.[37] We can estimate[32] the diffusivity, D_1, of the cores at the crossover point as $D_1 = R_c^2/2\tau$, where R_c is the particle jump length given by $R_c = \sqrt[3]{3V_c/(4\pi)}$, the hopping time $\tau \approx 1/\omega_c$, $V_c \approx (1 - \phi)\kappa T/G'(\omega_c)$, ϕ is the particle volume fraction, ω_c is the oscillatory frequency at which G' and G'' intersect, and T is the reference temperature at which the master curves are constructed. Using the data presented in Figure 3, this equation delivers $D_1 \sim 9.05 \times 10^{-26}$ m^2/s. Alternatively,[38] the diffusivity may be approximated from the Stokes−Einstein formula, $D_2 = \kappa T\omega_c/[6\pi R_p|G^*(\omega_c)|]$, where κ is the Boltzmann constant, R_p is the radius of core particles (~3.5 nm), and $|G^*(\omega_c)| = \sqrt{2G'^2(\omega_c)}$ is the absolute value of the complex modulus at ω_c. Using this equation, we find $D_2 \sim 5.77 \times 10^{-26}$ m^2/s. The nearly identical values of D_1 and D_2 indicate that the suggested meaning of the mechanical result for NOHM-I-PEI is plausible. Unfortunately, these values of D cannot be independently verified as they are far below the experimental limits of established techniques such as pulsed-field gradient NMR. Bourlinos *et al.*[32] have made an estimate of $\sim 10^{-15}$ m^2/s—a value that is just at the limit of what can be experimentally determined—for functionalized Si nanoparticles in a much less viscous medium.

We find that the low frequency slopes of G' and G'' are 0.96 and 0.79, respectively, for PEI, and 0.88 and 0.77 for NOHM-I-PEI. The slope of the glass-to-rubber transition region of G' and G'' *versus* ω as approximated by the Zimm model[39] is ~2/3 and is similar for many conventional polymers.[40] Simple molecular glass-forming liquids are expected to have single mechanical relaxation corresponding to the glass transition with low frequency slopes of 1 and 2 for G'' and G', respectively.[41] Evidently, the slopes obtained for both PEI and the hybrid material show intricate phenomena, not explained by these models, probably due, in part, to the highly branched nature of the polymer. Finally, the high-frequency limiting shear modulus, G_∞, is observed to slightly increase from 1.84×10^9 (PEI) to 2.45×10^9 Pa (NOHM-I-PEI), signifying mechanical enhancement in the latter material, evident also in the increased viscosity of the hybrid material (Figure S5).

BDS has the ability to probe molecular dynamics and charge transport in broad temperature and frequency ranges[42] making it a versatile tool for studying NOHMs. The technique measures the complex dielectric function, ε^*, which is equivalent to the complex conductivity function, σ^*. The two functions are related by the equation $\sigma^*(\omega,T) = i\varepsilon_0\omega\varepsilon^*(\omega,T)$, which means that $\varepsilon' = \sigma''/\omega\varepsilon_0$ and $\varepsilon'' = \sigma'/\omega\varepsilon_0$. Figure 4 shows dielectric loss (ε'') as a function of frequency as measured over heating and cooling runs for PEI and NOHM-I-PEI samples. The reproducibility of the measurements demonstrates thermal stability of the samples in the temperature range of interest. At high temperatures, the loss data has two peaks and a flank on the low-frequency side, while at lower temperatures, only one peak is present in the accessible frequency window. Evident from Figure 4 as well as Figure 5—which displays data over a wider temperature range and also includes the real part of the complex conductivity function—the differences between the measured spectra for PEI and NOHM-I-PEI are subtle.

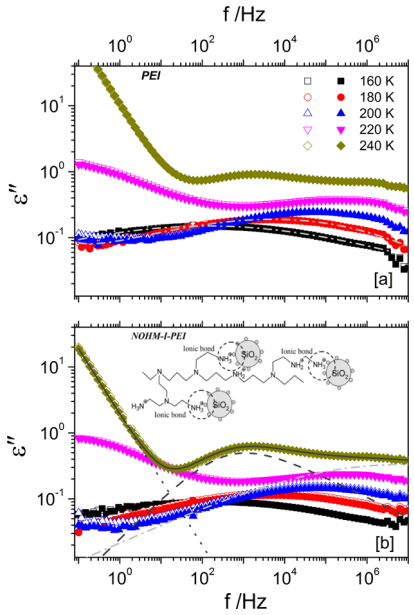

Figure 4. Dielectric loss as a function of frequency at different temperatures as shown for (a) neat highly-branched polyethylenimine (PEI) and (b) NOHM-I-PEI. At low temperatures, the data can be described by one Havriliak-Negami (HN) function as demonstrated in (a), while at higher temperatures, two HN functions are required—illustration shown for data taken at 240 K in (b). Filled and empty symbols represent data collected in cooling and heating runs, respectively. Inset: the chemical structure of NOHM-I-PEI obtained from Lin and Park.[13] The legend in panel (a) applies also for (b). The error bars are comparable to the size of the symbols unless otherwise indicated.

In order to quantitatively analyze the data, a combination of two Havriliak-Negami (HN)[43] functions and a term accounting for ionic conductivity contribution is used

https://dx.doi.org/10.1021/acs.macromol.0c02370
Macromolecules XXXX, XXX, XXX−XXX

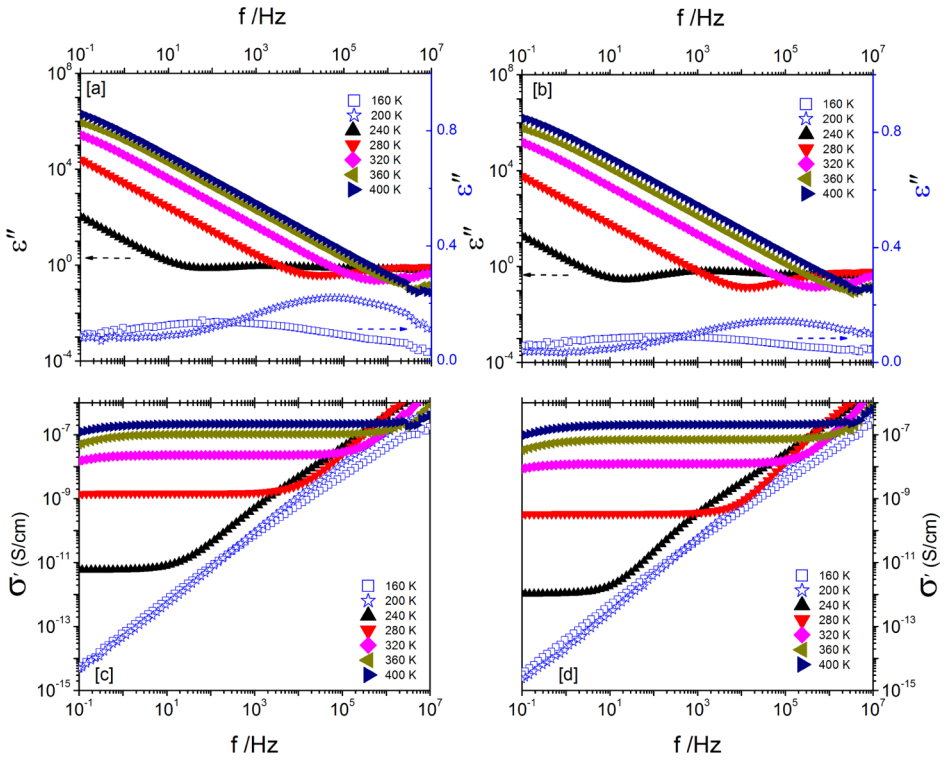

Figure 5. Imaginary part of the complex dielectric function $\varepsilon^*(f) = \varepsilon'(f) - i\varepsilon''(f)$ for (a) PEI and (b) NOHM-I-PEI, and the real part of the complex conductivity function $\sigma^*(f) = \sigma'(f) + i\sigma''(f)$ for (c) PEI and (d) NOHM-I-PEI. The error bars are comparable to the size of the symbols unless otherwise indicated.

$$\varepsilon^* = E_\infty + \left\{\frac{\Delta\varepsilon}{[1 + (i\omega\tau_{HN})^\beta]^\gamma}\right\}_{alpha} + \left\{\frac{\Delta\varepsilon}{[1 + (i\omega\tau_{HN})^\beta]^\gamma}\right\}_{beta} - i\left(\frac{\sigma_0}{\varepsilon_0\omega}\right)^s \quad (1)$$

where $\varepsilon^* = \varepsilon' - i\varepsilon''$ is the complex dielectric function, σ_0 is the d.c. ionic conductivity of the sample, ε_0 the dielectric permittivity of vacuum, ε_∞ the permittivity of the unrelaxed medium, $\Delta\varepsilon$ the dielectric relaxation strength, τ_{HN} the characteristic HN relaxation time, and β and γ are shape parameters accounting for symmetric and asymmetric broadening, respectively. Note that $\omega = 2\pi f$ is the angular frequency of the applied external field and $0 \leq s \leq 1$ is a scaling parameter. The subscripts α and β refer to the two dipolar relaxations observed in the systems under study. As demonstrated by the superposition of the fit function (dash-dotted lines in Figure 4a and the solid line in Figure 4b) to the measured data, this fitting procedure adequately describes the data.

First, we discuss the shape of the HN fit functions (for the primary structural relaxation) obtained from fitting the dielectric loss data to eq 1 above. Figure S6 shows HN functions normalized with respect to the maximum loss value as obtained at two select temperatures. It is observed that the peaks are broader for the polymer than the hybrid material, which is a rather counterintuitive finding given what is already known in traditional polymer nanocomposites.[44−46] This is however consistent with an observed broader T_g transition in the polymer than that in the NOHM material (Figure S2). Recently, it was demonstrated that broadening of the relaxation distribution times of the structural process in polymer-grafted nanocomposites can be understood to arise, in part, from an increase in free volume due to matrix-graft chain packing frustrations in the interfacial zones.[46] In the present system, the polymer is highly branched thereby increasing the likelihood of free volume in the neat system. In the hybrid material, no bulk free polymer matrix exists and we posit that the nanoparticles take up some of the available free volume. This effectively "freezes out" the fast modes that would otherwise be present due to the higher degrees of freedom to relax in the regions with voids. Additionally, as observed from the X-ray scattering data, the hybrid material has hierarchical structuring which includes mesoscale organization on a length scale of about 1.4 nm. It has been shown for other liquids that the dynamic signature of mesoscale organization is a Debye-like relaxation that is slower than the primary structural relaxation.[47] While a separate sub-α process is absent in the present system, the narrowing of the structural relaxation peak may be indicative of the contribution of mesoscale structures to the total polarization of the system. Further experimental and computational work on dynamics in NOHMs is needed to elucidate of this phenomenon.

To gain further insights from the fit functions, mean relaxation times, τ_m, were calculated from the HN parameters using the equation[42]

$$\tau_m(T) = \tau_{HN}\sin\left(\frac{\beta\gamma\pi}{2 + 2\gamma}\right)^{1/\beta}\sin\left(\frac{\beta\pi}{2 + 2\gamma}\right)^{-1/\beta} \quad (2)$$

and these are plotted as functions of inverse temperature in Figure 6. From the rheology data in Figure 3, the mean mechanical relaxation times were obtained using $\tau_m(T) = \tau_{ref}(T_{ref})/a_T$, where τ_{ref} is the mean structural relaxation time at the reference temperature T_{ref} and a_T is the corresponding shift

https://dx.doi.org/10.1021/acs.macromol.0c02370
Macromolecules XXXX, XXX, XXX−XXX

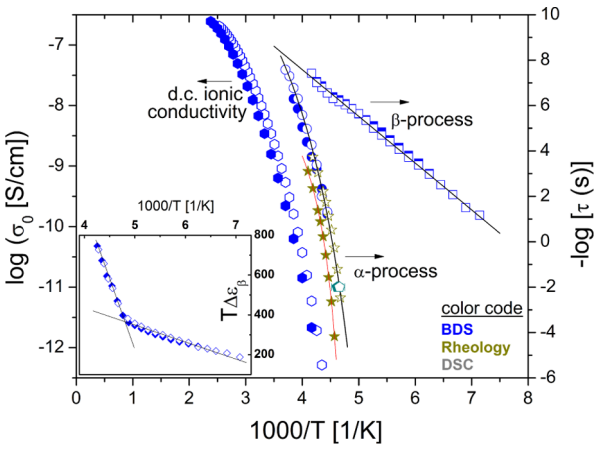

Figure 6. Mean relaxation times of the segmental (α-) and localized dipolar (β-) relaxations (right y-axis) for PEI and NOHM-I-PEI obtained from BDS (blue symbols) and rheology (dark yellow). The d.c. ionic conductivity (left y-axis) *versus* inverse temperature for the two samples (hexagons) is also presented. The T_g values determined from DSC are shown by pentagon symbols. Inset: evolution with temperature of the dielectric relaxation strength associated with the β-process in the neat polymer and the NOHM. In all cases, empty symbols are for PEI, while filled symbols represent NOHM-I-PEI data. The error bars are comparable to the size of the symbols unless otherwise indicated.

factor. Several pertinent observations can be made from this graph. First, as determined from BDS, the mean relaxation times for the two processes present in both neat PEI (empty blue symbols) and NOHM-I-PEI (filled blue symbols) coincide. Second, the process occurring at high temperatures has non-Arrhenius temperature activation and can be described (solid line) by the Vogel−Fulcher−Tammann (VFT) equation[48−50] ($\tau(T) = \tau_0 \exp(-DT_V/[T - T_V])$, where τ_0 and D are constants, and T_V is the Vogel temperature). Extrapolating the VFT fit to longer times, we observe that the mean relaxation time of 100 s occurs at 215 K, which is coincidentally also the calorimetrically determined glass transition temperature for the two samples. This coincidence is conventionally used[42] to unambiguously identify the primary structural (or segmental) relaxation, and we therefore assign this process to the fluctuation of just a few PEI segments, typically on a sub-nanometer length scale.[51] Third, the mean relaxation times obtained from rheology for PEI (open star symbols) agree with those determined by BDS helping buttress the argument that the process in question is indeed the segmental relaxation. However, the relaxation times from rheology for the NOHM (closed star symbols) are appreciably slower than those reported by dielectric spectroscopy. This likely arises from the fact that the measured times by rheology include additional contributions from the networks of the silica cores, as already discussed. Fourth, the relaxation at low temperatures exhibits an Arrhenius type of thermal activation which is fitted (see dashed line) by the function $\tau(T) = \tau_\infty \exp(-E_A/k_BT)$ (where τ_∞ is the relaxation time in the high temperature limit, k_B the Boltzmann constant, and E_A the activation energy). This is characteristic of localized fluctuations—so-called secondary dipolar relaxations. This process has an activation energy of about 37.9 kJ/mol and we specifically identify it as a β-process arising presumably from liberations of the amine-terminated side groups on the highly branched PEI. A similar molecular process has been observed in a composite comprising butadiene, styrene, and polyethyleneimine.[52] The temperature dependence of the dielectric relaxation strength, $\Delta\varepsilon_\beta$, of the β-process is depicted in the inset of Figure 6. It is observed that the slope of $T\Delta_\beta$ *versus* $1/T$ changes at T_g. We attribute this trend to the change in free volume that is known to occur at T_g, thereby presenting more degrees of freedom to the liberation motions of the amine-terminated side groups as the glass transition is traversed to higher temperatures. It has been demonstrated that the approach to the glassy state can be considered as being controlled *via* the linked contributions of free volume and temperature: upon gradual cooling, at T_g, a polymer melt can be said to have the minimum free volume that it must have to be still in the melt state.[53−55] For completeness, we note that this temperature dependence of the β-process can be explained without invoking the concept of free volume but instead by the idea of so-called cage breaking.[56−60] At low temperatures, the side group is pictured as undergoing local liberation motions while attached to static segments on the backbone. The restrictions imposed by static segments resemble those of a cage. As the temperature is increased, the segments begin to move and the cage becomes bigger thereby lending higher degrees of freedom to the side groups. Eventually the liberations of the side groups coordinate with segmental motion leading to a merger of the two relaxations at some finite temperature above T_g. Now, taking note of the identical temperature dependence and trend of $\Delta\varepsilon_\beta$, it is clear that the process has exactly the same origin and mechanism in both PEI and NOHM-I-PEI. Given the short length scales on which the α- and β-processes occur, it is no surprise that the presence of nanoparticles (in the NOHM) does not affect their mean relaxation rates. On the other hand, longer scale motions—such as the fluctuations of a chain's end-to-end vector—are slowed down, in dependence of molecular weight, as has been demonstrated for NOHMs comprising a canopy of Type A[61] polymers.[62]

We now turn our attention to long-range ionic conductivity in these samples. As observed in panels (c) and (d) of Figure 5, the real part of the complex conductivity exhibits a plateau at temperatures above 200 K in our frequency window. This plateau corresponds to the d.c. ionic conductivity, σ_0, of the sample. The decrease observed upon further lowering of the frequency (clearly seen at 360 and 400 K) is due to accumulation of charges at the electrodes—a phenomenon known as electrode polarization, which is outside the scope of the current study. We have extracted the values of σ_0 and plotted the same as functions of inverse temperature as shown in Figure 6. The absolute values of the d.c. ionic conductivity in both PEI and NOHM-I-PEI are rather low compared to standard ion conducting systems such as imidazolium-based ionic liquids which are characterized by values better than 10^{-5} S/cm at room temperature.[63] The levels of ionic conductivity observed here are typical for many amorphous polymers that basically arise from minute amounts of impurities left over from polymerization. However, given that ionic conductivity in the hybrid material is less than that of the neat polymer (following a similar trend as the respective viscosities—Figure S5), this can be deciphered to be proton conduction. The hydrogen bonds associated with NOHM-I-PEI cause a reduction in the number of protons contributing to long-range motion when compared to the case in neat PEI. This idea is worth being substantively tested using NOHMs based on ionic polymers such as polymerized ionic liquids in our future studies.

https://dx.doi.org/10.1021/acs.macromol.0c02370
Macromolecules XXXX, XXX, XXX−XXX

To obtain mechanistic understanding of the specific molecular motions associated with the relaxations probed by BDS, NMR was employed to explore local dynamics of the canopy. In particular, the spin−lattice relaxation of bulk PEI was compared to that of NOHM-I-PEI. Figure 7 presents the

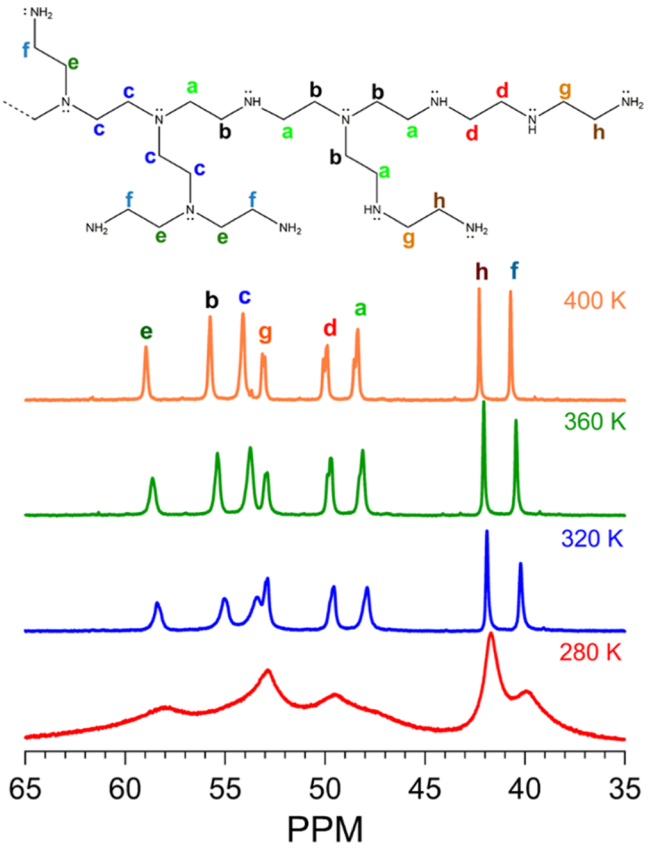

Figure 7. Scheme of the partial structure of the branched PEI (top) with alphabetic labels representing different methylene groups in the polymer chain. The ^{13}C NMR spectra (bottom) of neat, dry NOHM-I-PEI at different temperatures with the respective assignments.

carbon NMR spectra of NOHM-I-PEI at different temperatures (280−400 K). The spectra exhibit 8 distinguishable peaks which correspond to different methylene groups present in the polymer chain as indicated in the inset based on previous studies.[64−66] The ^{13}C chemical shift of a carbon atom can, therefore, be associated to the degree of branching of the nitrogen atoms in the α and β positions to the carbon atom. Peaks *a* and *b* are associated to methylene groups between a secondary and a tertiary amino group, where *a* is adjacent to the secondary and *b* to the tertiary groups. Peak *c* corresponds to a pair of equivalent methylene groups between two tertiary amino groups. Similarly, peak *d* is related to equivalent methylene groups between two secondary amino groups. Lastly, the pairs *e*-*f* and *g*-*h* are located between a tertiary and primary group and a secondary and primary group, respectively. Methylene groups *e*, *f*, *g*, and *h* would reflect, therefore, the relaxation of the extremities (either side or end chain) of the branched PEI canopy. Significant broadening of the peaks is observed as the temperature decreases. In particular, peaks *a* through *c*, associated with methylene groups located in the vicinity of tertiary amino groups in the polymer canopy, dramatically broaden as the temperature is decreased from 320 to 280 K to the point that these resonances are no longer visible as clear peaks in the spectrum but rather form a broad signal in the range between ∼70 and 50 ppm. This suggests that the mobility of these groups is significantly restrained in this lower temperature range. This effect is shown by the faster T_2^* relaxation time decay observed with the interior methylene group peaks (Figure S8).

Carbon-spin lattice relaxation times of the methylene groups were measured to obtain a more detailed picture of the dynamics of the pure PEI and tethered PEI (*i.e.,* NOHM-I-PEI) canopy in neat, dry samples. The spin−lattice relaxation time (T_1), also referred to as longitudinal relaxation time, was measured using the inversion recovery sequence. This sequence involves the determination of the rate constant for the relaxation of a spin system to its equilibrium magnetization immediately following perturbation from thermal equilibrium by a radio-frequency pulse.[31,67,68] T_1 values were determined for a range of temperatures (Figure 8). In both cases,

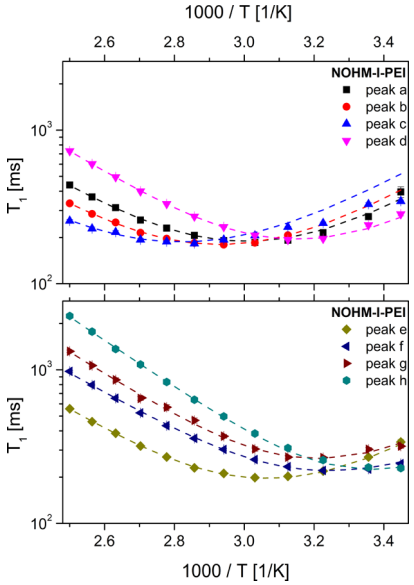

Figure 8. Plot of the relaxation times for the interior methylene groups (top) and exterior methylene groups (bottom) in NOHM-I-PEI as a function of temperature. The dashed lines are calculated from the estimated correlation times based on the BPP model.

temperature-dependent data exhibit a T_1 minimum. Such a minimum occurs at a temperature at which the molecular motions are near the observation frequency (100.1 MHz), subject to the condition $\omega\tau_c \sim 06.16$.[69] Figure 8 presents the results for the methylene groups located in the exterior of the polymer canopy (peaks *e*, *f*, *g*, and *h*) and those located in the backbone (peaks *a*, *b*, *c*, and *d*) in NOHM-I-PEI. From Figure 8, it is noticeable that for the methylene group located at the ends of the chains, the minimum occurs at lower temperatures than for the carbons located toward the interior of the canopy (Table 1). This shift suggests higher correlation time for the interior carbons. Therefore, the local motion is reduced for carbons located in the "interior" of the polymer chain in both PEI and NOHM-I-PEI. Comparing the behavior between PEI and NOHM-I-PEI for each particular methylene group, the similarity of the results in terms of shape (Figure S7) and temperature of the T_1 minimum (Table S1) is remarkable, which suggests that the molecular dynamics of the canopy is not sensitive to the presence of the silica cores. This outcome

https://dx.doi.org/10.1021/acs.macromol.0c02370
Macromolecules XXXX, XXX, XXX−XXX

Table 1. Activation Energies Estimated from the BPP and Arrhenius Model for the Neat PEI and NOHM-I-PEI Samples

	bPEI	NOHM-I-PEI
peak	E_a [kJ mol^{-1}]	E_a [kJ mol^{-1}]
a	25.81	25.52
b	25.39	25.16
c	22.26	23.72
d	26.51	26.50
e	26.46	26.15
f	25.68	24.93
g	28.71	27.59
h	29.39	29.50

agrees with previous reports on NOHM systems[31] and with our BDS results.

To further explore the relaxation process, the correlation times can be extracted from the relaxation times through the Bloembergen-Purcell-Pound (BPP) model $\frac{1}{T_1} = C\left(\frac{\tau_C}{1+\omega_0^2\tau_C^2} + \frac{4\tau_C}{1+4\omega_0^2\tau_C^2}\right)$, in which the relaxation rate is related to the correlation time τ_c with C and ω_0 constant.[70] This approach has been described previously.[69] The temperature dependence of the correlation time is represented by an Arrhenius relationship in this analysis, allowing the estimation of the activation energies. The dashed lines in Figure 8 correspond to the relaxation time calculated from the correlation times for the NOHM-I-PEI. In general, the fitting shows a good agreement with the acquired data for the peaks associated with methylene groups in the vicinity of primary amino groups, which would correspond to the side and end groups of the canopy (peaks *e*, *f*, *g*, and *h*) and those located between two secondary amino groups (peak *d*). This implies that the local dynamics can be described by one mode of motion. The relaxation of these exterior methylene groups agrees with the β-process identified from the BDS analysis in terms of the activation energy. The most significant deviations are observed for the peaks associated with methylene groups (peaks *a*, *b*, and *c*) in the vicinity of tertiary amino groups. This could be due to a deviation from an Arrhenius behavior, as suggested for the α process from BDS, or can be caused by the significant broadening of such peaks at low temperatures. The resulting activation energies for each peak in the PEI and NOHM-I-PEI cases are listed in Table 1. Although bulk PEI exhibits slightly higher activation energies, the magnitudes are very similar for all the analyzed peaks.

The temperature range sampled differs for the BDS and NMR experiments. However, it is clear that extrapolating the temperature-dependent BDS data in Figure 6 to the range of temperatures used in the NMR experiments would yield rough agreement with correlation time values on the order of 10^{-9} s. Although the α and β processes are not readily distinguished by BDS in the NMR temperature range, it is also notable that the α process, which we associate with the "interior" carbons of the chain, has a much stronger temperature dependence than does the β process. This is in accordance with the significant extra broadening of the NMR lines from these carbons. Thus, the NMR results complement those obtained by BDS and provide insights into the specific moieties involved in local and segmental relaxations in both the neat polymer and the NOHMs. These results demonstrate the significant roles played by the inorganic core and polymeric canopy in determining the local and collective dynamics in this class of hybrid materials.

CONCLUSIONS

We have synthesized and characterized molecular dynamics in nanoparticle organic hybrid materials comprising silica nanoparticles as the core and highly branched polyethylenimine as the canopy. For comparison, neat polyethylenimine is also studied. We show that the NOHMs retain liquid-like behaviors with the rates of its structural and secondary relaxations exactly identical to those of the neat constituent polymer as revealed by BDS and NMR. However, the presence of nanoparticles in the system does increase the viscosity of NOHM-I-PEI relative to PEI. While the increased viscosity is not often favored, the enhanced chemical and thermal stability of tethered polymers in NOHMs provides a great potential for a wide range of reactive and separation systems including flow batteries and CO_2 capture. The findings from this study highlight the key role played by the canopy in determining the properties of these hybrid materials and suggest that the choice of the polymer used as canopy is critical in achieving the desired properties.

ASSOCIATED CONTENT

Supporting Information

The Supporting Information is available free of charge at https://pubs.acs.org/doi/10.1021/acs.macromol.0c02370.

shift factors and viscosity data (rheology) and T_1 and T_2^* relaxation times (NMR) (PDF)

AUTHOR INFORMATION

Corresponding Authors

Thomas A. Zawodzinski, Jr. − *Department of Chemical and Biomolecular Engineering, University of Tennessee, Knoxville, Tennessee 37996-2200, United States; Oak Ridge National Laboratory, Oak Ridge, Tennessee 37831, United States;* orcid.org/0000-0002-2690-8784; Email: tzawodzi@utk.edu

Ah-Hyung Alissa Park − *Department of Earth and Environmental Engineering, Department of Chemical Engineering, Lenfest Center for Sustainable Energy, Columbia University, New York 10027-6699, United States;* Email: apark@ei.columbia.edu

Joshua Sangoro − *Department of Chemical and Biomolecular Engineering, University of Tennessee, Knoxville, Tennessee 37996-2200, United States;* orcid.org/0000-0002-5483-9528; Email: jsangoro@utk.edu

Authors

Emmanuel Urandu Mapesa − *Department of Chemical and Biomolecular Engineering, University of Tennessee, Knoxville, Tennessee 37996-2200, United States;* orcid.org/0000-0002-2206-0990

Nelly M. Cantillo − *Department of Chemical and Biomolecular Engineering, University of Tennessee, Knoxville, Tennessee 37996-2200, United States;* orcid.org/0000-0002-9616-4135

Sara T. Hamilton − *Department of Earth and Environmental Engineering, Department of Chemical Engineering, Lenfest Center for Sustainable Energy, Columbia University, New York 10027-6699, United States*

https://dx.doi.org/10.1021/acs.macromol.0c02370
Macromolecules XXXX, XXX, XXX−XXX

Matthew A. Harris − *Department of Chemical and Biomolecular Engineering, University of Tennessee, Knoxville, Tennessee 37996-2200, United States*

Complete contact information is available at: https://pubs.acs.org/10.1021/acs.macromol.0c02370

Author Contributions

The manuscript was written through contributions of all authors.

Notes

The authors declare no competing financial interest.

■ ACKNOWLEDGMENTS

This work was supported as part of the Breakthrough Electrolytes for Energy Storage (BEES), an Energy Frontier Research Center funded by the U.S. Department of Energy, Office of Science, Basic Energy Sciences under Award #: DE-SC0019409. E.U.M. acknowledges partial financial support from the National Science Foundation, Division of Materials Research, Polymers Program, through DMR-1905597. M.A.H. acknowledges financial support by the National Science Foundation, the Division of Chemistry through no. CHE-1753282. The rheology measurements were conducted at the Oak Ridge National Laboratory's Center for Nanophase Materials Sciences, which is sponsored by the Division of Scientific User Facilities, Office of Basic Energy Sciences, U.S. Department of Energy. SAXS measurements were performed at the Shared Materials Instrumentation Facility (SMIF) at Duke University. We thank Thomas Kinsey and Jonathan Coote for fruitful discussions.

■ REFERENCES

(1) Kim, D.; Archer, L. A. Nanoscale Organic-Inorganic Hybrid Lubricants. *Langmuir* **2011**, *27*, 3083−3094.

(2) Moganty, S. S.; Jayaprakash, N.; Nugent, J. L.; Shen, J.; Archer, L. A. Ionic-Liquid-Tethered Nanoparticles: Hybrid Electrolytes. *Angew Chem. Int. Ed. Engl.* **2010**, *49*, 9158−9161.

(3) Warren, S. C.; Banholzer, M. J.; Slaughter, L. S.; Giannelis, E. P.; DiSalvo, F. J.; Wiesner, U. B. Generalized Route to Metal Nanoparticles with Liquid Behavior. *J. Am. Chem. Soc.* **2006**, *128*, 12074−12075.

(4) Voevodin, A. A.; et al. Nanoparticle-Wetted Surfaces for Relays and Energy Transmission Contacts. *Small* **2007**, *3*, 1957−1963.

(5) Patton, S. T.; Voevodin, A. A.; Vaia, R. A.; Pender, M.; Diamanti, S. J.; Phillips, B. Nanoparticle Liquids for Surface Modification and Lubrication of Mems Switch Contacts. *J. Microelectromech. Syst.* **2008**, *17*, 741−746.

(6) Park, S. I.; Lim, J. H.; Kim, J. H.; Yun, H. I.; Roh, J. S.; Kim, C. G.; Kim, C. O. Effects of Surfactant on Properties of Magnetic Fluids for Biomedical Application. *Phys. Status Solidi B* **2004**, *241*, 1662−1664.

(7) Morais, P. C.; Santos, J. G.; Silveira, L. B.; Gansau, C.; Buske, N.; Nunes, W. C.; Sinnecker, J. P. Susceptibility Investigation of the Nanoparticle Coating-Layer Effect on the Particle Interaction in Biocompatible Magnetic Fluids. *J. Magn. Magn. Mater.* **2004**, *272−276*, 2328−2329.

(8) Kim, I.; Svendsen, H. F. Comparative Study of the Heats of Absorption of Post-Combustion Co2 Absorbents. *Int. J. Greenhouse Gas Control* **2011**, *5*, 390−395.

(9) Shin, J. Y.; Lee, B. S.; Jung, Y.; Kim, S. J.; Lee, S.-g. Palladium Nanoparticles Captured onto Spherical Silica Particles Using a Urea Cross-Linked Imidazolium Molecular Band. *Chem. Commun.* **2007**, 5238−5240.

(10) Ma, Z.; Yu, J.; Dai, S. Preparation of Inorganic Materials Using Ionic Liquids. *Adv. Mater.* **2010**, *22*, 261−285.

(11) Park, Y.; Shin, D.; Jang, Y. N.; Park, A.-H. A. Co2 Capture Capacity and Swelling Measurements of Liquid-Like Nanoparticle Organic Hybrid Materials Via Attenuated Total Reflectance Fourier Transform Infrared Spectroscopy. *J. Chem. Eng. Data* **2011**, *57*, 40−45.

(12) Park, Y.; Petit, C.; Han, P.; Alissa Park, A.-H. Effect of Canopy Structures and Their Steric Interactions on Co2 Sorption Behavior of Liquid-Like Nanoparticle Organic Hybrid Materials. *RSC Adv.* **2014**, *4*, 8723.

(13) Lin, K.-Y. A.; Park, A.-H. A. Effects of Bonding Types and Functional Groups on Co2 Capture Using Novel Multiphase Systems of Liquid-Like Nanoparticle Organic Hybrid Materials. *Environ. Sci. Technol.* **2011**, *45*, 6633−6639.

(14) Yang, Y.; Zhang, Z. G.; Grulke, E. A.; Anderson, W. B.; Wu, G. Heat Transfer Properties of Nanoparticle-in-Fluid Dispersions (Nanofluids) in Laminar Flow. *Int. J. Heat Mass Transfer* **2005**, *48*, 1107−1116.

(15) Murshed, S. M. S.; Leong, K. C.; Yang, C. A Model for Predicting the Effective Thermal Conductivity of Nanoparticle-Fluid Suspensions. *Int. J. Nanosci.* **2006**, *05*, 23−33.

(16) Jang, S. P.; Choi, S. U. S. Role of Brownian Motion in the Enhanced Thermal Conductivity of Nanofluids. *Appl. Phys. Lett.* **2004**, *84*, 4316−4318.

(17) Jwo, C.-S.; Teng, T.-P.; Chang, H. A Simple Model to Estimate Thermal Conductivity of Fluid with Acicular Nanoparticles. *J. Alloys Compd.* **2007**, *434−435*, 569−571.

(18) Wang, X.; Xu, X.; Choi, S. U. S. Thermal Conductivity of Nanoparticle - Fluid Mixture. *J. Thermophys. Heat Transfer* **1999**, *13*, 474−480.

(19) Eastman, J. A.; Choi, S. U. S.; Li, S.; Yu, W.; Thompson, L. J. Anomalously Increased Effective Thermal Conductivities of Ethylene Glycol-Based Nanofluids Containing Copper Nanoparticles. *Appl. Phys. Lett.* **2001**, *78*, 718−720.

(20) Pil Jang, S.; Choi, S. U. S. Effects of Various Parameters on Nanofluid Thermal Conductivity. *J. Heat Transfer* **2007**, *129*, 617−623.

(21) Bourlinos, A. B.; Ray Chowdhury, S.; Herrera, R.; Jiang, D. D.; Zhang, Q.; Archer, L. A.; Giannelis, E. P. Functionalized Nanostructures with Liquid-Like Behavior: Expanding the Gallery of Available Nanostructures. *Adv. Funct. Mater.* **2005**, *15*, 1285−1290.

(22) Bourlinos, A. B.; Herrera, R.; Chalkias, N.; Jiang, D. D.; Zhang, Q.; Archer, L. A.; Giannelis, E. P. Surface-Functionalized Nanoparticles with Liquid-Like Behavior. *Adv. Mater.* **2005**, *17*, 234−237.

(23) Andrew Lin, K.-Y.; Park, Y.; Petit, C.; Park, A.-H. A. Thermal Stability, Swelling Behavior and Co2 Absorption Properties of Nanoscale Ionic Materials (Nims). *RSC Adv.* **2014**, *4*, 65195−65204.

(24) Lin, K.-Y. A.; Petit, C.; Park, A.-H. A. Effect of So2 on Co2 Capture Using Liquid-Like Nanoparticle Organic Hybrid Materials. *Energy Fuels* **2013**, *27*, 4167−4174.

(25) Petit, C.; Lin, K.-Y. A.; Park, A.-H. A. Design and Characterization of Liquidlike Poss-Based Hybrid Nanomaterials Synthesized Via Ionic Bonding and Their Interactions with Co2. *Langmuir* **2013**, *29*, 12234−12242.

(26) Park, Y.; Decatur, J.; Lin, K.-Y. A.; Park, A.-H. A. Investigation of Co2 Capture Mechanisms of Liquid-Like Nanoparticle Organic Hybrid Materials Via Structural Characterization. *Phys. Chem. Chem. Phys.* **2011**, *13*, 18115−18122.

(27) Yu, W.; Wang, T.; Park, A.-H. A.; Fang, M. Toward Sustainable Energy and Materials: Co2 Capture Using Microencapsulated Sorbents. *Ind. Eng. Chem. Res.* **2020**, *59*, 9746−9759.

(28) Wang, J.; Fang, W.; Luo, J.; Gao, M.; Wan, Y.; Zhang, S.; Zhang, X.; Park, A.-H. A. Selective Separation of Co2 Using Novel Mixed Matrix Membranes Based on Pebax and Liquid-Like Nanoparticle Organic Hybrid Materials. *J. Membr. Sci.* **2019**, *584*, 79−88.

(29) Yu, W.; Wang, T.; Park, A.-H. A.; Fang, M. Review of Liquid Nano-Absorbents for Enhanced Co2 Capture. *Nanoscale* **2019**, *11*, 17137−17156.

(30) Cantillo, N. M.; Bruce, M.; Hamilton, S. T.; Feric, T. G.; Park, A.-H. A.; Zawodzinski, T. A. Electrochemical Behavior of Copper Ion Complexed with Nanoparticle Organic Hybrid Materials. *J. Electrochem. Soc.* **2020**, *167*, 116508.
(31) Jespersen, M. L.; Mirau, P. A.; Meerwall, E. v.; Vaia, R. A.; Rodriguez, R.; Giannelis, E. P. Canopy Dynamics in Nanoscale Ionic Materials. *ACS Nano* **2010**, *4*, 3735−3742.
(32) Bourlinos, A. B.; Giannelis, E. P.; Zhang, Q.; Archer, L. A.; Floudas, G.; Fytas, G. Surface-Functionalized Nanoparticles with Liquid-Like Behavior: The Role of the Constituent Components. *Eur. Phys. J. E Soft Matter* **2006**, *20*, 109−117.
(33) Sharma, K. P.; Choudhury, C. K.; Srivastava, S.; Davis, H.; Rajamohanan, P. R.; Roy, S.; Kumaraswamy, G. Assembly of Polyethyleneimine in the Hexagonal Mesophase of Nonionic Surfactant: Effect of Ph and Temperature. *J. Phys. Chem. B* **2011**, *115*, 9059−9069.
(34) Liu, X.; Abel, B. A.; Zhao, Q.; Li, S.; Choudhury, S.; Zheng, J.; Archer, L. A. Microscopic Origins of Caging and Equilibration of Self-Suspended Hairy Nanoparticles. *Macromolecules* **2019**, *52*, 8187−8196.
(35) Pakula, T.; Vlassopoulos, D.; Fytas, G.; Roovers, J. Structure and Dynamics of Melts of Multi Polymer Stars. *Macromolecules* **1998**, *31*, 8931−8940.
(36) Agarwal, P.; Qi, H.; Archer, L. A. The Ages in a Self-Suspended Nanoparticle Liquid. *Nano Lett.* **2010**, *10*, 111−115.
(37) Cheng, S.; et al. Big Effect of Small Nanoparticles: A Shift in Paradigm for Polymer Nanocomposites. *ACS Nano* **2017**, *11*, 752−759.
(38) Mason, T. G. Estimating the Viscoelastic Moduli of Complex Fluids Using the Generalized Stokes-Einstein Equation. *Rheol. Acta* **2000**, *39*, 371−378.
(39) Rubinstein, M.; Colby, R. H. *Polymer Physics*; Oxford University Press: London, 2003.
(40) Choi, U. H.; Ye, Y.; Salas de la Cruz, D.; Liu, W.; Winey, K. I.; Elabd, Y. A.; Runt, J.; Colby, R. H. Dielectric and Viscoelastic Responses of Imidazolium-Based Ionomers with Different Counterions and Side Chain Lengths. *Macromolecules* **2014**, *47*, 777−790.
(41) Wyss, H. M. *Fluids, Colloids and Soft Materials: An Introduction to Soft Matter Physics*; John Wiley & Sons, Inc: Hoboken, NJ, 2016.
(42) Kremer, F.; Schönhals, A. *Broadband Dielectric Spectroscopy*; Springer: Berlin, 2003.
(43) Havriliak, S.; Negami, S. A Complex Plane Representation of Dielectric and Mechanical Relaxation Processes in Some Polymers. *Polymer* **1967**, *8*, 161−210.
(44) Füllbrandt, M.; Purohit, P. J.; Schönhals, A. Combined Ftir and Dielectric Investigation of Poly(Vinyl Acetate) Adsorbed on Silica Particles. *Macromolecules* **2013**, *46*, 4626−4632.
(45) Gong, S.; Chen, Q.; Moll, J. F.; Kumar, S. K.; Colby, R. H. Segmental Dynamics of Polymer Melts with Spherical Nanoparticles. *ACS Macro Lett.* **2014**, *3*, 773−777.
(46) Mapesa, E. U.; Street, D. P.; Heres, M. F.; Kilbey, S. M.; Sangoro, J. Wetting and Chain Packing across Interfacial Zones Affect Distribution of Relaxations in Polymer and Polymer-Grafted Nanocomposites. *Macromolecules* **2020**, *53*, 5315−5325.
(47) Cosby, T.; Vicars, Z.; Wang, Y.; Sangoro, J. Dynamic-Mechanical and Dielectric Evidence of Long-Lived Mesoscale Organization in Ionic Liquids. *J. Phys. Chem. Lett.* **2017**, *8*, 3544−3548.
(48) Fulcher, G. S. Analysis of Recent Measurements of the Viscosity of Glasses - Reprint. *J. Am. Chem. Soc.* **1992**, *75*, 1043−1055.
(49) Tammann, G.; Hesse, W. Die Abhängigkeit Der Viscosität Von Der Temperatur Bie Unterkühlten Flüssigkeiten. *Z. Anorg. Allg. Chem.* **1926**, *156*, 245−257.
(50) Vogel, H. The Law of the Relationship between Viscosity of Liquids and the Temperature. *Phys. Z.* **1921**, *22*, 645−646.
(51) Bahar, I.; Erman, B.; Kremer, F.; Fischer, E. W. Segmental Motions of Cis-Polyisoprene in the Bulk State: Interpretation of Dielectric Relaxation Data. *Macromolecules* **1992**, *25*, 816−825.
(52) Kolesov, I. S. Effect of Phase Separation on Dielectric Relaxation and Electrical Conductivity of the Butadiene-Styrene Rubber-Polyethyleneimine System. *Polym. Sci.* **1987**, *29*, 1059−1063.
(53) White, R. P.; Lipson, J. E. G. Polymer Free Volume and Its Connection to the Glass Transition. *Macromolecules* **2016**, *49*, 3987−4007.
(54) Doolittle, A. K. Studies in Newtonian Flow. Ii. The Dependence of the Viscosity of Liquids on Free-Space. *J. Appl. Phys.* **1951**, *22*, 1471−1475.
(55) White, R. P.; Lipson, J. E. G. Free Volume in the Melt and How It Correlates with Experimental Glass Transition Temperatures: Results for a Large Set of Polymers. *ACS Macro Lett.* **2015**, *4*, 588−592.
(56) Caporaletti, F.; Capaccioli, S.; Valenti, S.; Mikolasek, M.; Chumakov, A. I.; Monaco, G. A Microscopic Look at the Johari-Goldstein Relaxation in a Hydrogen-Bonded Glass-Former. *Sci. Rep.* **2019**, *9*, 14319.
(57) Khodadadi, S.; Sokolov, A. P. Protein Dynamics: From Rattling in a Cage to Structural Relaxation. *Soft Matter* **2015**, *11*, 4984−4998.
(58) Lappala, A.; Sefton, L.; Fenimore, P. W.; Terentjev, E. M. Connectivity and Free-Surface Effects in Polymer Glasses. *Sci. Rep.* **2019**, *9*, 3830.
(59) Smith, G. D.; Bedrov, D. Relationship between the A- and B-Relaxation Processes in Amorphous Polymers: Insight from Atomistic Molecular Dynamics Simulations of 1,4-Polybutadiene Melts and Blends. *J. Polym. Sci., Part B: Polym. Phys.* **2007**, *45*, 627−643.
(60) Yu, H.-B.; Yang, M.-H.; Sun, Y.; Zhang, F.; Liu, J.-B.; Wang, C. Z.; Ho, K. M.; Richert, R.; Samwer, K. Fundamental Link between Beta Relaxation, Excess Wings, and Cage-Breaking in Metallic Glasses. *J. Phys. Chem. Lett.* **2018**, *9*, 5877−5883.
(61) Stockmayer, W. H. Dielectric Dispersion in Solutions of Flexible Polymers. *Pure Appl. Chem.* **1967**, *15*, 539−554.
(62) Kim, S. A.; Mangal, R.; Archer, L. A. Relaxation Dynamics of Nanoparticle-Tethered Polymer Chains. *Macromolecules* **2015**, *48*, 6280−6293.
(63) Sangoro, J. R.; Iacob, C.; Serghei, A.; Friedrich, C.; Kremer, F. Universal Scaling of Charge Transport in Glass-Forming Ionic Liquids. *Phys. Chem. Chem. Phys.* **2009**, *11*, 913−916.
(64) Lukovkin, G. M.; Pshezhetsky, V. S.; Murtazaeva, G. A. Nmr 13c Study of the Structure of Polyethyleneimine. *Eur. Polym. J.* **1973**, *9*, 559−565.
(65) Pierre, T. S.; Geckle, M. 13-Nmr Analysis of Branched Polyethyleneimine. *J. Macromol. Sci., Chem.* **1985**, *22*, 877−887.
(66) Holycross, D. R.; Chai, M. Comprehensive Nmr Studies of the Structures and Properties of Pei Polymers. *Macromolecules* **2013**, *46*, 6891−6897.
(67) Friebolin, H. *Basic One- and Two-Dimensional NMR Spectroscopy*, 2005.
(68) Claridge, T. D. W. High-Resolution Nmr Techniques in Organic Chemistry. *High-resolution Nuclear Magnetic Resonance Techniques in Organic Chemistry*, 1999.
(69) Gouverneur, M.; Jeremias, S.; Schönhoff, M. 7li Nuclear Magnetic Resonance Studies of Dynamics in a Ternary Gel Polymer Electrolyte Based on Polymeric Ionic Liquids. *Electrochim. Acta* **2015**, *175*, 35−41.
(70) Bloembergen, N.; Purcell, E. M.; Pound, R. V. Relaxation Effects in Nuclear Magnetic Resonance Absorption. *Phys. Rev.* **1948**, *73*, 679−712.

https://dx.doi.org/10.1021/acs.macromol.0c02370
Macromolecules XXXX, XXX, XXX−XXX

SUPPORTING INFORMATION

for:

Localized and Collective Dynamics in liquid-like Polyethylenimine-based Nanoparticle Organic Hybrid Materials

Emmanuel Urandu Mapesa[1], Nelly M. Cantillo[1], Sara T. Hamilton[2], Matthew A. Harris[1], Thomas A. Zawodzinski Jr.*[1,3], Ah-Hyung Alissa Park*[2] and Joshua Sangoro*[1]

[1]Department of Chemical and Biomolecular Engineering, University of Tennessee, Knoxville, TN 37996-2200

[2]Department of Earth and Environmental Engineering, Department of Chemical Engineering, Lenfest Center for Sustainable Energy, Columbia University, New York, NY 10027-6699

[3]Oak Ridge National Laboratory, Oak Ridge, Tennessee 37831, United States

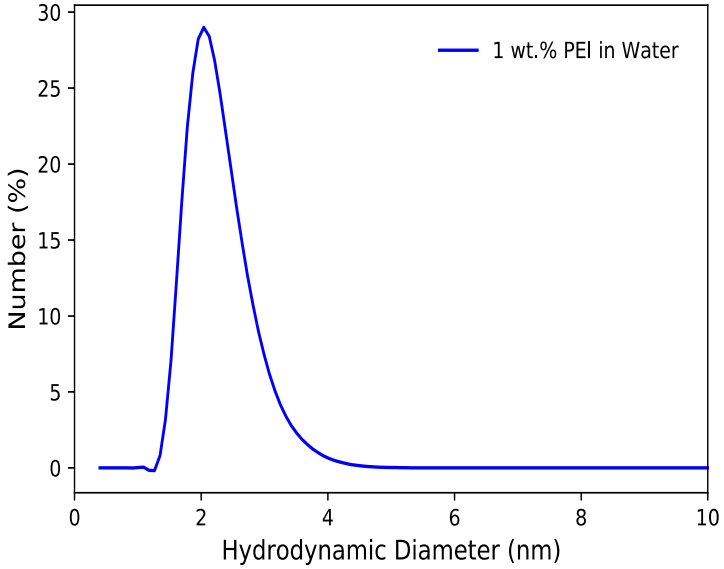

Figure S1: Hydrodynamic Diameter number distribution of 1 wt.% PEI in water measured via dynamic light scattering (DLS) at 25 °C.

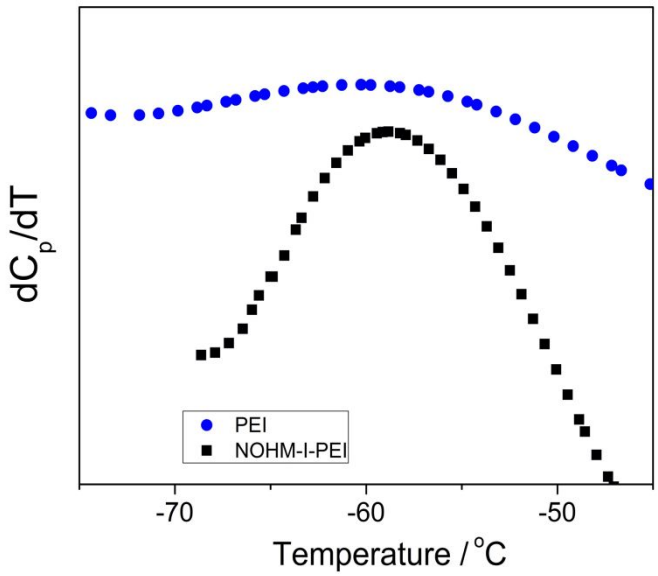

Figure S2: Derivative plots of the DSC traces showing the Tg and breadth of the transition in PEI and NOHM-I-PEI. Evidently, the hybrid material has a narrower peak than the neat polymer.

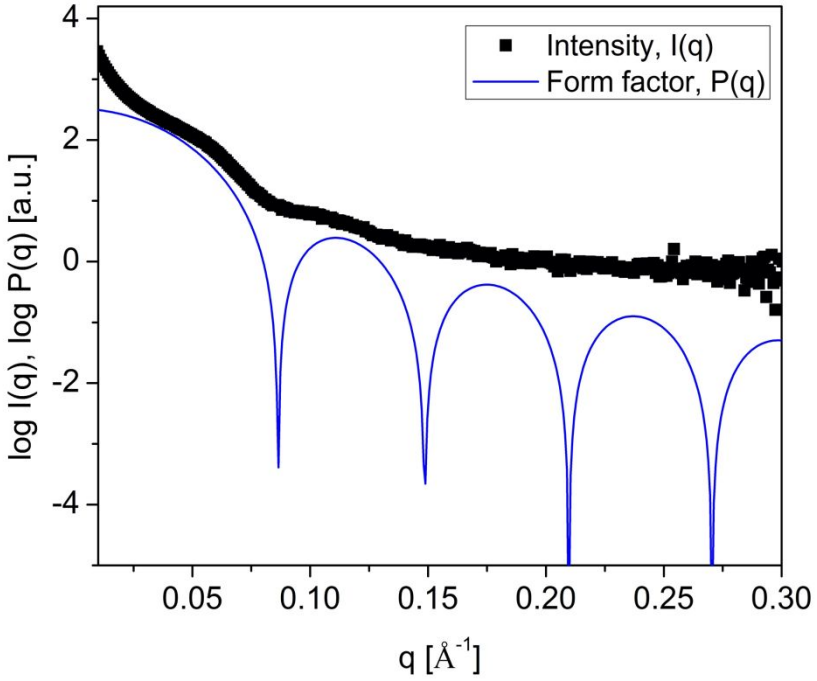

Figure S3. SAXS profile of the NOHM-I-PEI studied in this work. The symbols indicate the experimental data while the solid line is a simple form factor model[1] for monodisperse spheres, $P(q) = k\left[3\frac{\sin(qR) - qR\cos(qR)}{(qR)^3}\right]^2$, offset by a scaling factor, k, modeled by adjusting the radius, R, of the sphere until it matches the oscillatory nature of the data. q is the momentum transfer. The radius of the sphere is found to be 5.2 nm.

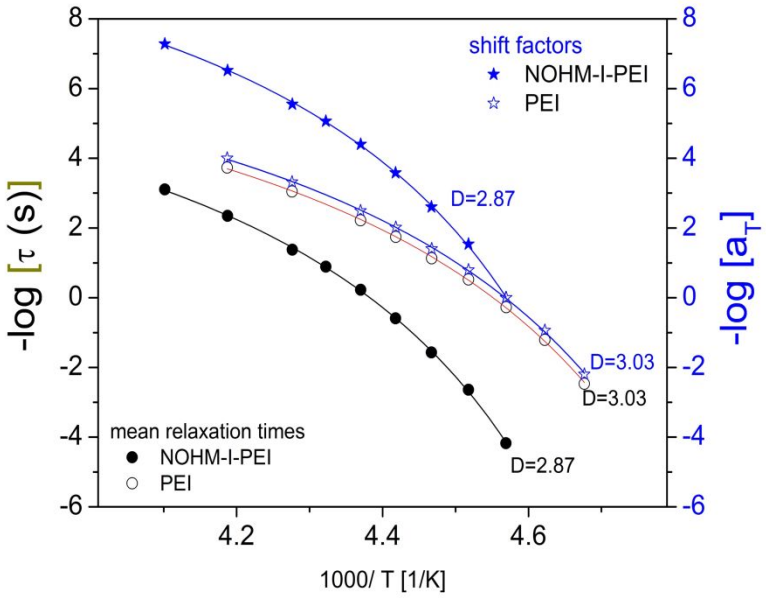

Figure S4. Temperature dependence of the mean relaxation times (circles) determined from rheology, and of the shift factors (stars) used to plot the master curves in Figures 3 and S5. The lines represent fits to the data using the VFT equation (see text in the main manuscript). Values of the parameter D (which is a measure of the extent of deviation from Arrhenius dependence) are shown for each fit function. Evidently, the shift factors have the same temperature dependence as the corresponding mean relaxation times. The other fit parameters are: solid stars (τ_0 = 9e12 s, T_0 = 199.1 K); empty stars (τ_0 = 2.3e9 s, T_0 = 191.9 K); solid circles (τ_0 = 6.2e8 s, T_0 = 199.1 K); and empty circles (τ_0 = 1.2e9 s, T_0 = 191.9 K).

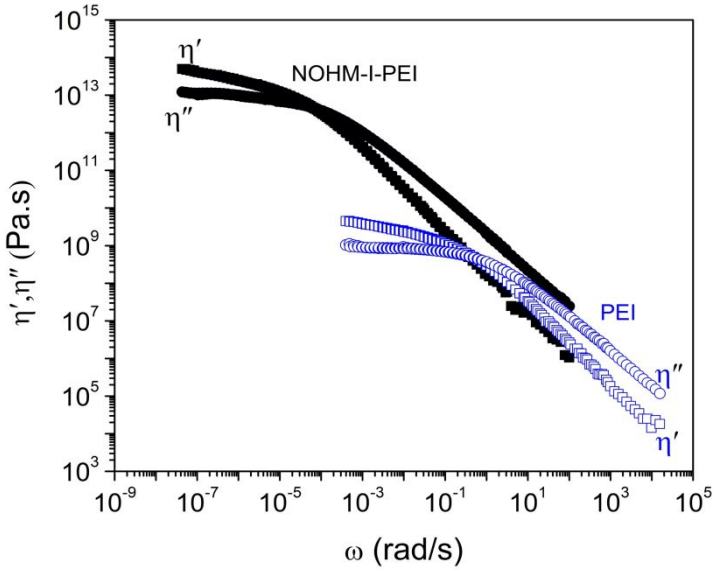

Figure S5. Master curves (reference temperature, - 55°C) showing the real (η′) and imaginary (η″) parts of the complex viscosity, η*, for PEI (blue symbols) and NOHM-I-PEI (back symbols). The error bars are comparable to the size of the symbols unless otherwise indicated.

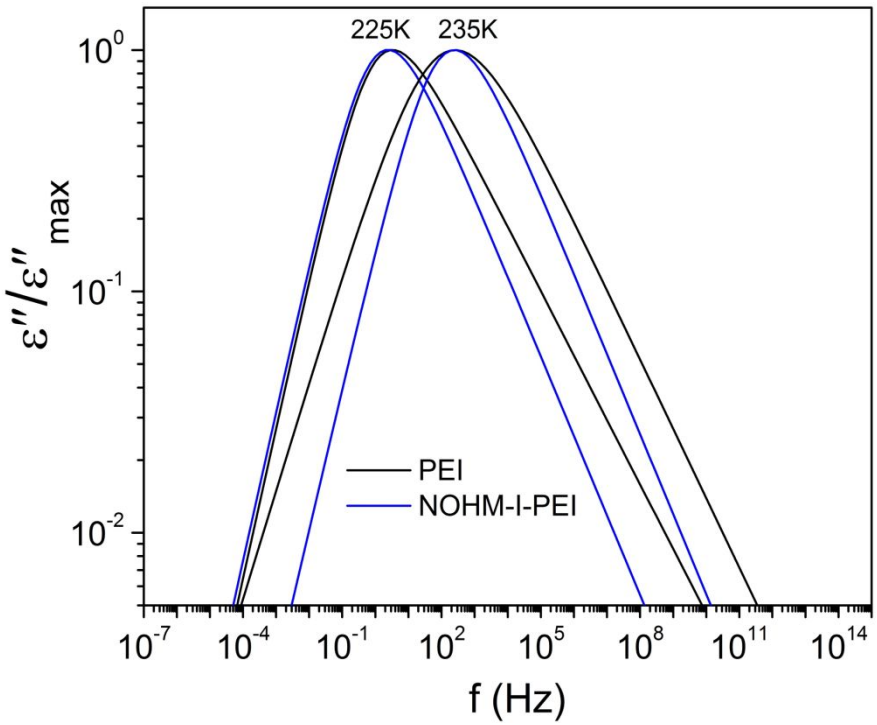

Figure S6: HN functions used to describe the structural relaxation in the polymer (PEI) and the hybrid material (NOHM-I-PEI) at two select temperatures.

Figure S7 compares the temperature dependence of the carbon T_1's for the peaks *d* and *h* (Figure 7) in the neat PEI and the NOHM-I-PEI canopy. The trends observed in Figure S6 are representative of the results obtained with all the identified carbon in the PEI chain. The most remarkable feature of this plot is that the relaxation times (and molecular dynamics) of the methylene groups do not seem to be sensitive to the presence of the silica core. This agrees with the results obtained with BDS.

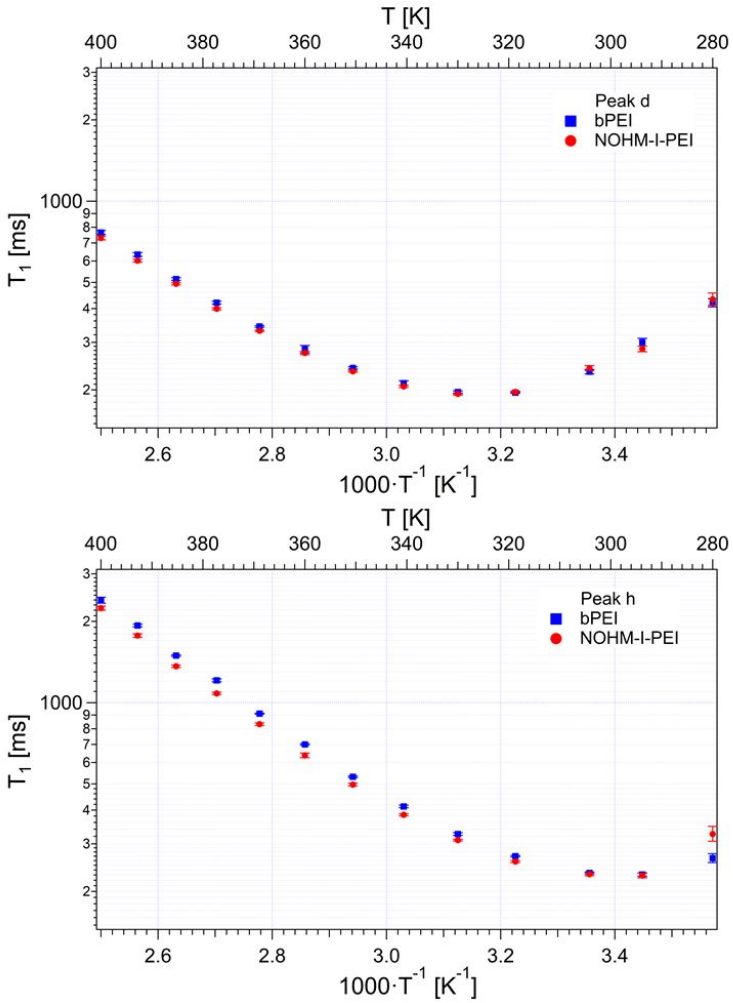

Figure S7. Plot of the T_1 relaxation times for peak d (Top) peak h (bottom) in the neat PEI and NOHM-I-PEI canopy as a function of temperature.

The carbon T_1 minimum occurs when the molecular motions are near the observation frequency (100.64 MHz). From Figure S7, it is noticeable that in the methylene group located in the end of the chain (peak h) the minimum occurs at a lower temperature than the carbon located towards the interior of the canopy (Peak *d*). This comparison is observed with all the identified exterior methylene groups (peaks *e* to *h*) (Table S1). This shift suggests an increase in the correlation time. The local motion is reduced for carbons located in the 'interior' of the polymer canopy in both the unbound and tethered cases.

Transverse or T_2^* relaxation times were calculated from the estimation of the half-weight line-width ($\Delta\nu_{1/2}$) for each ^{13}C peak. The term T_2^* includes the contributions from static magnetic field inhomogeneities throughout the sample volume, and the 'genuine' or 'natural' transverse relaxation processes (T_2) arising from intramolecular and intermolecular interactions in the sample[2]. For exponential relaxation, T_2^* can be calculated from the equation $\Delta\nu_{1/2} = \frac{1}{\pi T_2^*}$. Plots of the estimated T_2^* relaxation times as a function of temperature are shown in Figure S8. In general, the interior carbons (peaks *a* to *d*) exhibit a faster T_2^* relaxation time decay as temperature decreases.

Table S1. Estimated temperatures at the T_1 minimum for the branched PEI and NOHM-I-PEI.

	bPEI		NOHM-I-PEI	
Peak	T @ $T_{1,min}$ [K]	T^{-1} @ $T_{1,min}$ [K^{-1}]	T @ $T_{1,min}$ [K]	T^{-1} @ $T_{1,min}$ [K^{-1}]
a	330.47	3.03	329.92	3.03
b	341.88	2.92	340.07	2.94
c	353.28	2.83	350.18	2.86
d	316.60	3.16	316.80	3.16
e	324.44	3.08	326.42	3.08
f	304.64	3.28	304.73	3.06
g	312.12	3.20	310.64	3.22
h	293.65	3.40	297.17	3.36

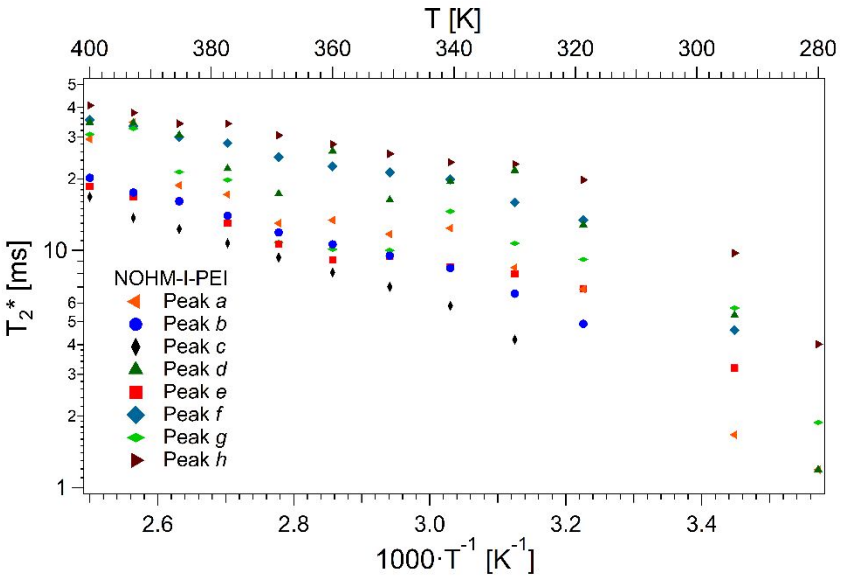

Figure S8. Plot of the T_2 relaxation for the NOHM-I-PEI canopy as a function of temperature.

References

1. Dulle, M.; Jaber, S.; Rosenfeldt, S.; Radulescu, A.; Forster, S.; Mulvaney, P.; Karg, M., Plasmonic gold-poly(N-isopropylacrylamide) core-shell colloids with homogeneous density profiles: a small angle scattering study. *Phys Chem Chem Phys* **2015,** *17* (2), 1354-67.
2. Claridge, T., *NMR Techniques in Organic Chemistry*. Pergamon: Oxford, 1999; Vol. 19, p 381.